Magn Reson Med Sci 2021; 20; 264–271
doi:10.2463/mrms.mp.2019-0134
Published Online: August 21, 2020

MAJOR PAPER

# Histologic Distribution and Characteristics on MR Imaging of Ultrasmall Superparamagnetic Iron Oxide in Ethyl-nitrosourea-induced Endogenous Rat Glioma

Atsuko Yamamoto[1], Kai Takaki[2], Shigehiro Morikawa[3], Kiyoshi Murata[2], and Ryuta Ito[2*]

**Purpose:** (1) To evaluate the enhancement patterns of an ultrasmall superparamagnetic iron oxide contrast agent (USPIO-CA) compared with those of a gadolinium-based contrast agent (Gd-BCA). (2) To compare the histologic distribution of USPIO-related iron particles (USPIO-IPs) with the USPIO-enhancement area in the early vascular and in the cellular imaging phase (E- and L-phase, respectively) after intravenous CA administration.

**Methods:** We performed USPIO-enhanced MRI of *N*-ethyl-*N*-nitrosourea (ENU)-induced endogenous rat glioma, including spin-echo (SE) $T_1$-weighted images ($T_1$WIs) and gradient-recalled-echo (GRE) $T_2$-weighted images ($T_2$WIs), before and at 3–6 h after USPIO-CA administration for E-phase images. For L-phase images, MRI was performed at 16–19 and 62–69 h after administration. Two observers determined the USPIO-enhancement area on E-phase images and Gd-enhancement areas. We compared the USPIO-enhancement size (USPIO-ES) and Gd-ES on SE $T_1$WIs, and the hypo-intense USPIO-ES on GRE $T_2$WIs and Gd-ES using the Wilcoxon signed-rank test. In addition, two raters visually evaluated the correspondence between the histologic distribution of USPIO-IPs and the USPIO-enhancement area on corresponding GRE $T_2$WIs at each phase using a 3-rating scale.

**Results:** Significantly smaller hyper-intense, hypo-intense and combined hyper-/hypo-intense areas were observed on USPIO-enhanced SE $T_1$WIs compared with Gd-enhanced images (all $P < 0.001$). The hypo-intense USPIO-ES on GRE $T_2$WIs was significantly smaller than the Gd-ES ($P = 0.001$). The distribution of USPIO-IPs on histopathological specimen and USPIO-enhancement on GRE $T_2$WIs exhibited poor agreement in 5 of 9 tumors with enhancement from rats sacrificed early. The distribution of microglia containing USPIO-IPs corresponded with the pattern of USPIO-enhancement in the 2 tumors with late enhancement.

**Conclusion:** The enhancement pattern and size of USPIO-CA in a rat glioma model were statistically different from those of Gd-BCA. Our histological data suggests that USPIO-enhanced MRI offers vascular bed imaging in E-phase and might depict the intra-tumoral distribution of immune effector cells in L-phase.

**Keywords:** *ultrasmall superparamagnetic iron oxide contrast agent, rat glioma, histological correlation*

## Introduction

Gliomas are common primary brain tumors and sometimes show aggressive behavior with a very poor prognosis.[1] Clinically, contrast-enhanced (CE) MRI using gadolinium-based contrast agents (Gd-BCAs) enables evaluation of the aggressiveness of gliomas by assessing vascular factors of the tumors, such as the intra-tumoral vascular bed volume and degree of blood–brain barrier (BBB) disruption.[2,3]

Ultrasmall superparamagnetic iron oxide (USPIO) particles have been developed for use as a contrast agent in CE MRI.[4–11] These nanoparticles are based on magnetite ($Fe_3O_4$)

[1]Department of Radiology, KOHKA Public Hospital, Koka, Shiga, Japan
[2]Department of Radiology, Shiga University of Medical Science, Otsu, Shiga, Japan
[3]Molecular Neuroscience Research Center, Shiga University of Medical Science, Otsu, Shiga, Japan
[*]Corresponding author: Department of Radiology, Shiga University of Medical Science, Seta Tsukinowacho, Otsu, Shiga 520-2192, Japan. Phone: +81-77-548-2536, Fax: +81-77-544-0986, E-mail: itoh@belle.shiga-med.ac.jp



Received: September 25, 2019 | Accepted: June 14, 2020

or maghemite ($\gamma Fe_2O_3$) cores coated with materials such as dextran, which range from 10 to 50 nm in hydrodynamic diameter.[9] Human clinical studies and experiments involving murine glioma models have revealed some attractive features of USPIO contrast agents (USPIO-CAs) when compared with Gd-BCAs.[6–10] Furthermore, because Gd-BCAs pose the risk of nephrogenic systemic fibrosis in patients with severe renal dysfunction and have recently been reported to result in Gd-deposition in the brain, USPIO-CAs have attracted interest as an MR contrast agent.[11] Since USPIO-CAs remain in the intravascular space due to their relatively larger particle size compared with Gd-BCAs, dynamic MRI using USPIO-CAs may provide more accurate vascular parameters than dynamic MRI using Gd-BCAs.[7–10] This may enable more accurate determination of tumor grade and monitoring of the efficacy of antiangiogenic chemotherapy. As well as intravascular contrast agents, another interesting application of USPIO-CAs is in cellular imaging. The USPIOs are ingested by phagocytic cells such as reactive astrocytes including microglia. Microglia play an important role in glioma progression and are an attractive target for multi-modal therapy targeting malignant gliomas.[12] Therefore, CE MRI with USPIO-CAs is a novel technique, which shows potential for monitoring the immune environment and immunotherapy of gliomas.[6,9]

We performed sequential USPIO-enhanced MRI of a rat glioma model to evaluate the early vascular imaging phase (E-phase) and the late cellular imaging phase (L-phase) following intravenous USPIO-CA administration. Since we used a rat *N*-ethyl-*N*-nitrosourea (ENU)-induced endogenous glioma model, despite difficulties in controlling tumor behavior including location, size, and grading, we eliminated the potential for artificial modification of inflammatory reactions caused by implantation or grafting of tumors. Therefore, we could simulate the complex immune environment of brain tumors more accurately than the exogenous models used in previous reports.[13] The purpose of this study was to elucidate whether USPIO-CA is a valid alternative to Gd-BCA in medical MRI by evaluating the following: (i) tumor enhancement patterns revealed by USPIO-CAs compared with Gd-BCAs, (ii) time course of the enhancement patterns on various sequences and (iii) time course of histologic localization of USPIO-IPs.

## Materials and Methods

### *Animal model*

Tumors were induced in Fischer 344 rats (CLEA Japan, Tokyo, Japan) by transplacental exposure of litters to ENU (50 mg/kg; 20 mg/mL in 0.2M phosphate-buffered saline [PBS]; N85109-5G, Sigma-Aldrich Japan, Tokyo, Japan). The study was performed on 20 offspring rats aged 4–8 months. To check induced tumor development, rats were initially imaged at 3 months of age and then every 1 or 2 weeks depending on tumor size. All experiments complied with the National Institute of Health's Guide for the Care and Use of Laboratory Animals and the Animal Care Guidelines of our institution.

### *Magnetic resonance imaging*

We used a horizontal 7-Tesla MR scanner (Unity Inova VnmrJ 1.1c; Agilent, Santa Clara, CA, USA) with a superconducting magnet with a 40-cm clear bore (7.0-T/400 mm; Japan Superconductor Technology, Kobe, Japan) and a 12-cm bore actively shielded gradient coil capable of producing magnetic field gradients up to 400 mT/m (Magnex Scientific Ltd., Abingdon, UK). A 43-mm-diameter homemade coil was used to receive radiofrequency.

Rats were anesthetized during imaging procedures using 2.0–2.5% isoflurane in 40% oxygen and 60% room air through a mask covering the nose. Their heads were tightly fixed with sponge packed in the coil.

### *Pre-contrast baseline and Gd-enhanced MRI*

A set of 3 sequences (each including 14 images with a section thickness of 1.2 mm, intersectional gap of 0.2 mm, FOV of 30 × 30 mm and matrix size of 256 × 128) was obtained to establish pre-contrast baseline images from a total of 20 rats (weight 160–380 g). The sequences and their parameters were as follows: spin-echo (SE) $T_2$-weighted images ($T_2$WIs) (TR of 2500 ms; TE of 18 ms; average [AVE] of 2), gradient-recalled-echo (GRE) $T_2$WIs (TR/TE = 600/8; flip angle [FA] = 30.0°; AVE = 2), and SE $T_1$-weighted images ($T_1$WIs) (TR/TE = 850/12; AVE = 2). Subsequently, rats were intravenously injected with 0.4 mmol/kg body weight of Gd-BCA (Gadodiamide Hydrate [Omniscan], Daiichi-Sankyo, Tokyo, Japan), and Gd-enhanced SE $T_1$WIs were obtained with the same acquisition parameters as the pre-contrast baseline SE $T_1$WIs.

### *USPIO-enhanced MRI*

Three of the 20 rats were not injected with USPIO-CA to create a control group. The remaining 17 rats were injected intravenously with 10 mg Fe/kg body weight of USPIO-CA (neutral surface charge carboxydextran-coated magnetite with a particle diameter of 25–40 nm supplied by Meito Sangyo, Aichi, Japan) on the following day to allow sufficient time for Gd-BCA clearance. The USPIO-enhanced images were obtained using the same acquisition parameters as for pre-contrast images 3–6 h following USPIO-CA administration for E-phase imaging from the 17 rats and at 16–19 and 62–69 h following USPIO-CA administration for L-phase imaging in 7 rats. Rats were returned to their cages after each imaging session following USPIO-CA administration. Rats were randomly assigned to the control group, the group in which the rats were sacrificed after E-phase imaging, and the group in which the rats were sacrificed after L-phase imaging.

### *Histopathology*

Following MRI, rats were sacrificed under deep anesthesia by intraperitoneal administration of sodium pentobarbital (150 mg/kg body weight), and 4% paraformaldehyde and 0.25% glutaraldehyde in 0.1M PBS were perfused through the heart. The brains were removed and sliced to match the

location of histologic specimens with those of the MR images. We cut at 3 µm sections and mounted them on glass slides. Sections were stained with Prussian blue to determine the localization of iron oxide, and cell spots were counter-stained with Nuclear Fast Red. To detect microglia, specimens were stained with anti-Iba1 antibody diluted 1:1000 (FUJIFILM Wako Pure Chemical, Osaka, Japan), using the conventional ABC method (Elite ABC kit, Vector Laboratories, Burlingame, CA, USA). The reaction product was developed using diaminobenzidine. Histochemical images were obtained from micrographs using image-processing software (cellSens Dimension; Olympus, Tokyo, Japan).

## *Analysis*

### Time course of USPIO-enhancement

We evaluated intra-tumoral USPIO-enhancement on USPIO-enhanced SE $T_1$WIs and GRE $T_2$WIs at 3–6, 16–19, and 62–69 h following USPIO-CA administration by comparing USPIO-enhanced MR images with the matching pre-contrast MR images. Two observers (R.I. and K.T.) visually reviewed the images and determined the number of tumors with USPIO-enhancement by mutual consent.

### Comparison of early-phase intra-tumoral enhancement size by USPIO-CA and Gd-BCA

We measured the intra-tumoral USPIO-enhancement sizes (USPIO-ESs) on USPIO-enhanced SE $T_1$WIs and GRE $T_2$WIs. The Gd-enhancement sizes (Gd-ESs) were measured on Gd-enhanced SE $T_1$WIs. Two observers manually drew regions of interest (ROIs) and delineated the areas of enhancement with increased or decreased signal intensity on all image sections covering the tumor area using NIH ImageJ 1.52a software. We calculated the enhancement-positive area by subtracting enhancement-negative areas from the total area that was delineated within the outer edge of the enhancement territory using "ROI Manager" tool (Fig. 1).

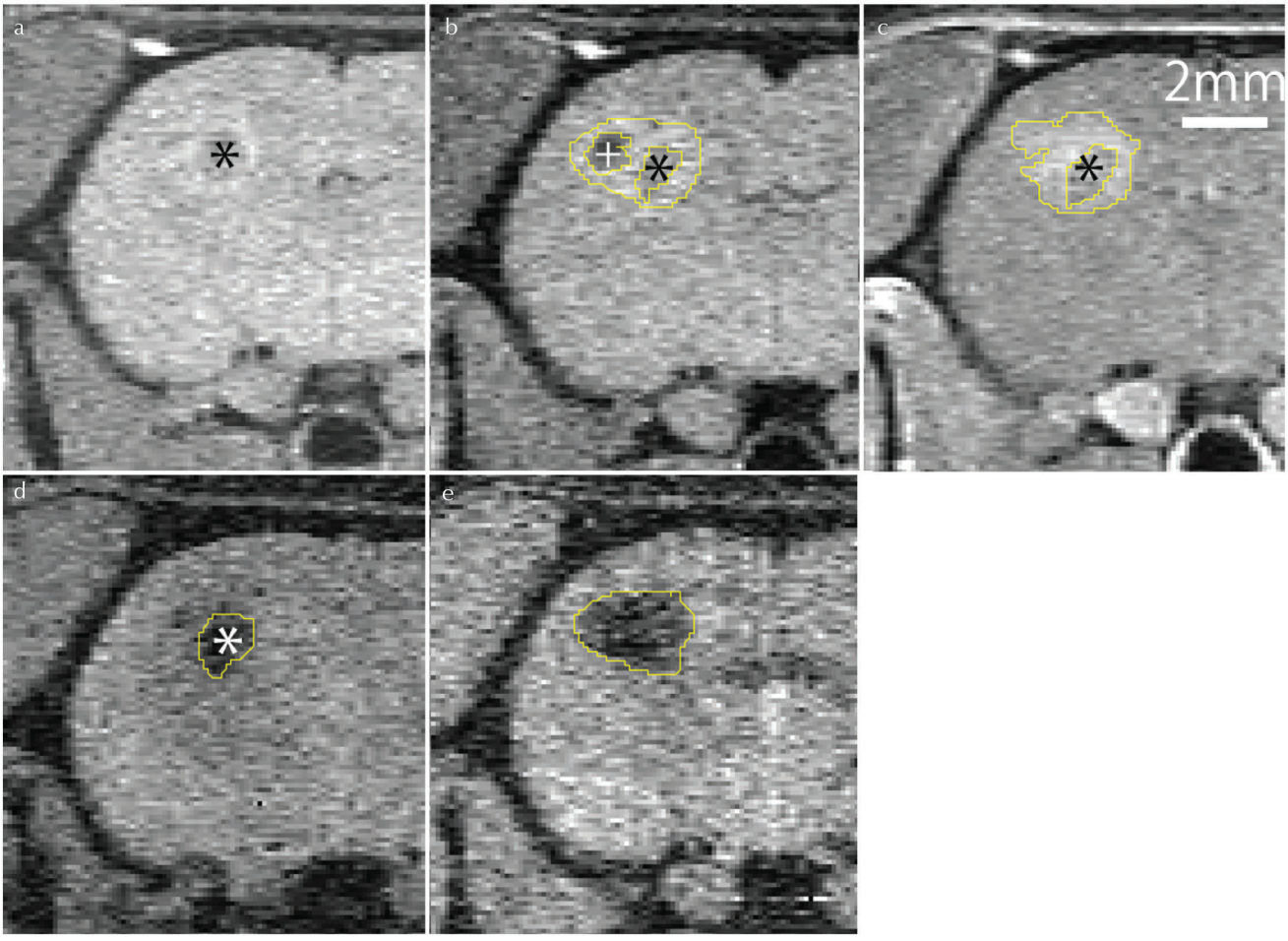


**Fig. 1** ROI measurement in early-phase USPIO-enhanced and Gd-enhanced MR images of an ENU-induced tumor. SE $T_1$WIs obtained (**a**) pre-contrast and (**b**) 3 h following administration of USPIO-CA. (**c**) Gd-enhanced image. Gradient-recalled-echo images obtained (**d**) pre-contrast and (**e**) 3 h following administration of USPIO-CA. Hypo-intense intra-tumoral pre-existent hemorrhage (asterisks in **a**–**d**) and enhancement areas were manually segmented (yellow ROIs in **b**–**e**). Hypo-intense enhancement is demonstrated on USPIO-enhanced spin-echo $T_1$WI (+ in **b**). CA, contrast agent; ENU, N-ethyl-N-nitrosourea; ROI, region of interest; SE, spin-echo; $T_1$WI, $T_1$-weighted image; USPIO, ultrasmall superparamagnetic iron oxide. (Color version is available online)

Interobserver agreement was assessed by calculating the intraclass correlation coefficients. Based on the excellent interobserver agreement, the mean value of the two measurements was used. We compared hyper- or hypo-intense USPIO-ES on SE $T_1$WIs with Gd-ES on Gd-enhanced $T_1$WIs, as well as the summation of hyper- or hypo-intense USPIO-ESs and Gd-ES, and compared hypo-intense USPIO-ES on GRE $T_2$WIs with Gd-ES, using the Wilcoxon signed-rank test. Statistical analyses were performed using SPSS software version 25 (IBM, Armonk, NY, USA).

**Histological correlation between distribution of USPIO-related iron particles and enhancement extent**

Two raters (R.I. and A.Y.) evaluated whether the location of iron oxide spots stained with Prussian blue matched the intra-tumoral USPIO-enhancement on GRE $T_2$WIs by using a 3-rating scale: good, fair or poor. The distribution of these spots and iron-loaded microglia on the histochemical images were documented in a descriptive manner.

## Results

We induced 26 tumors in 20 rats, including 4 in 3 control rats, using ENU. The 3 control rats which did not receive USPIO-CA were sacrificed just after pre-contrast baseline and Gd-enhanced MR imaging. Ten rats with 12 tumors were sacrificed at 3–6 h after USPIO-CA administration (early sacrificed), and 7 rats with 10 tumors were sacrificed 62–69 h after USPIO-CA administration (late sacrificed). Two of the 12 tumors from the early sacrificed rats, and 3 of the 10 tumors from the late sacrificed rats were not included in analysis due to severe signal loss on GRE $T_2$WIs or damaged histological sections. Ultimately, 10 tumors from eight early sacrificed rats and 7 from the six late sacrificed rats were included for analysis.

### *Pre-existent hemorrhage*

Non-contrast GRE $T_2$WIs revealed hypo-intense areas within all 4 tumors from control rats. Histology revealed that iron-particles originating from intra-tumoral hemorrhage were scattered within the hypo-intense areas on corresponding GRE $T_2$WIs. We therefore assumed that the hypo-intense areas within tumors observed on pre-contrast GRE $T_2$WIs in subsequent evaluations were due to pre-existing hemorrhage and eliminated hypo-intense (pre-existent hemorrhage) areas on the corresponding pre-contrast baseline GRE $T_2$WIs from hypo-intense areas on USPIO-enhanced images when USPIO-ES with decreased signal intensity was observed (Fig. 1).

**Time course of USPIO-enhancement**

The number of tumors that exhibited changes in signal intensity on SE $T_1$WIs and GRE $T_2$WIs at each time point following USPIO-CA administration are summarized in Table 1. On USPIO-enhanced SE $T_1$WIs, 11 of 17 tumors demonstrated USPIO-enhancement with various signal intensity changes in E-phase (Figs. 2 and 3). Three tumors exhibited both hyper- and hypo-intense areas. In L-phase images, obtained at 16–19 and 62–69 h following USPIO-CA administration, hypo-intense enhancement remained in 2 tumors (Fig. 3).

Intra-tumoral hypo-intense enhancement was observed on USPIO-enhanced GRE $T_2$WIs. In E-phase, 14 of the 17 tumors from early and late sacrificed rats exhibited decreased signal intensity (Figs. 2 and 3). Two of the seven tumors from late sacrificed rats showed hypo-intense enhancement (Fig. 3); these 2 also exhibited hypo-intense enhancement on USPIO-enhanced $T_1$WIs in the L-phase.

**Comparison of E-phase intra-tumoral enhancement size using USPIO-CA and Gd-BCA**

The data exhibited excellent interobserver agreement with an intraclass correlation coefficient of 0.995 (95% confidence interval, 0.988–0.997). Mean enhancement sizes determined by the two observers are detailed in Table 1. The intra-tumoral hyper- and/or hypo-intense USPIO-ES on SE $T_1$WIs and the hypo-intense USPIO-ES on GRE $T_2$WIs were significantly smaller than Gd-ES. Furthermore, the total of hyper- or hypo-intense USPIO-ES on SE $T_1$WIs was significantly smaller than the hypo-intense USPIO-ES on GRE $T_2$WIs.

**Histological correlation between distribution of USPIO-related iron particles and enhancement extent**

The number of tumors in early sacrificed rats which showed a good, fair, and poor correlation between USPIO-IP distribution on histologic images and USPIO-enhancement extent on GRE $T_2$WIs were 1, 3, and 5, respectively. We identified USPIO-IPs on the wall of cavitation in the tumor and in extravascular interstitial spaces (Fig. 2). In the two tumors of late sacrificed rats that exhibited late enhancement, USPIO-IPs were distributed within the USPIO-enhancement area (Fig. 3). The USPIO-IP distribution reflected the USPIO-enhancement area in those tumors. Most USPIO-IPs were observed to be located within the cellular space of Iba1-positive cells (Fig. 3).

## Discussion

The present study shows that enhancement patterns and ES measured on USPIO-enhanced SE $T_1$WIs and GRE $T_2$WIs are different from those on Gd-enhanced SE $T_1$WIs in rat ENU-induced glioma. On USPIO-enhanced SE $T_1$WIs, we identified intra-tumor hyper- and/or hypo-intense enhancement where Gd-enhanced $T_1$WIs showed simply hyper-intense enhancement. Furthermore, the total size of hypo- or hyper-intense enhancement was significantly smaller when measured on USPIO-enhanced SE $T_1$WIs. The differences in the particle size and BBB permeability of the two agents may be one reason for the discrepancies, and iso-intense USPIO-enhancement with signal intensity that is equal to that on

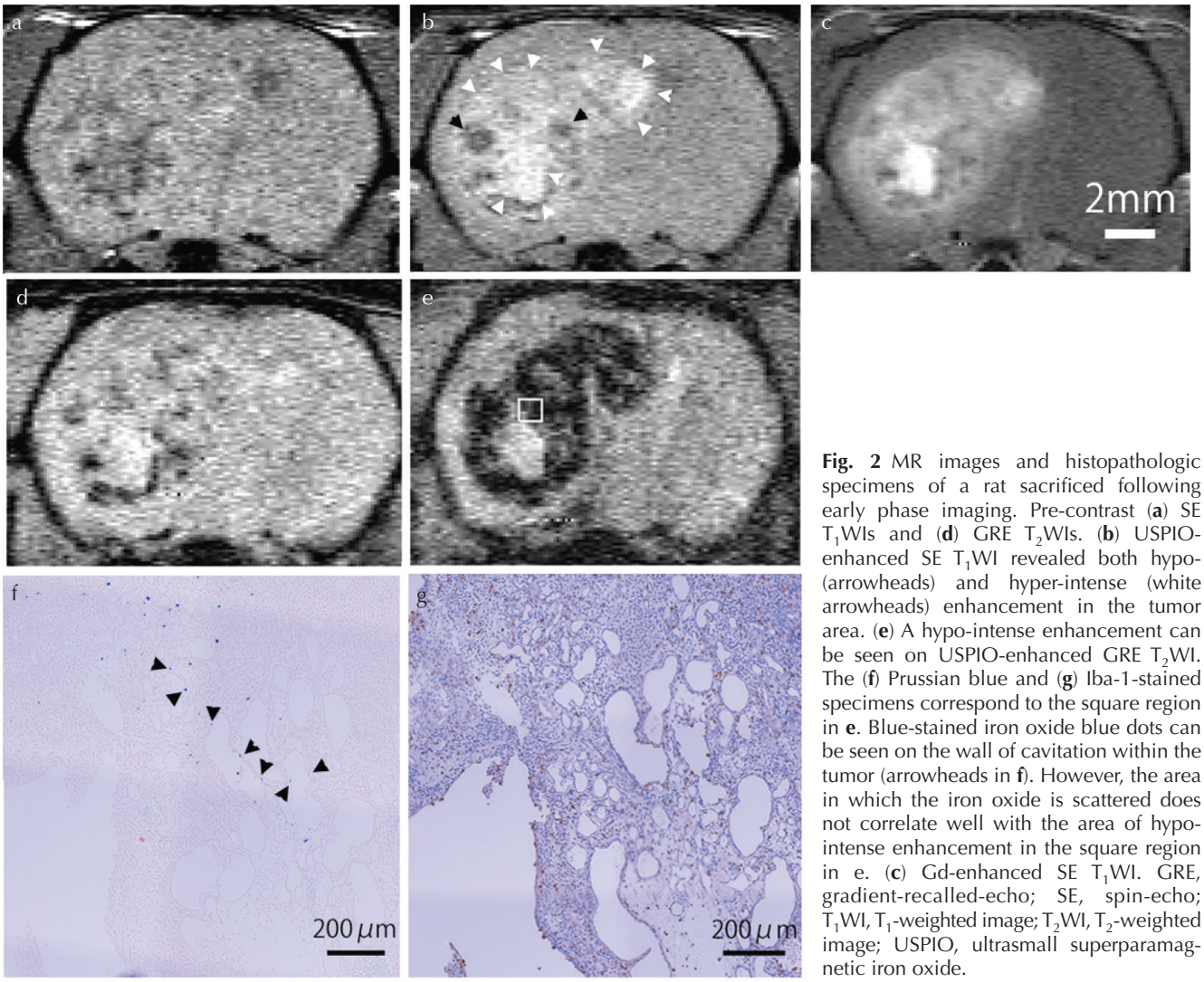


**Fig. 2** MR images and histopathologic specimens of a rat sacrificed following early phase imaging. Pre-contrast (**a**) SE $T_1$WIs and (**d**) GRE $T_2$WIs. (**b**) USPIO-enhanced SE $T_1$WI revealed both hypo- (arrowheads) and hyper-intense (white arrowheads) enhancement in the tumor area. (**e**) A hypo-intense enhancement can be seen on USPIO-enhanced GRE $T_2$WI. The (**f**) Prussian blue and (**g**) Iba-1-stained specimens correspond to the square region in **e**. Blue-stained iron oxide blue dots can be seen on the wall of cavitation within the tumor (arrowheads in **f**). However, the area in which the iron oxide is scattered does not correlate well with the area of hypo-intense enhancement in the square region in e. (**c**) Gd-enhanced SE $T_1$WI. GRE, gradient-recalled-echo; SE, spin-echo; $T_1$WI, $T_1$-weighted image; $T_2$WI, $T_2$-weighted image; USPIO, ultrasmall superparamagnetic iron oxide.

pre-contrast tumor images may also contribute. It has been reported that USPIO-enhanced $T_1$WIs exhibit decreased and increased signal intensity in areas of high and low concentration of contrast agent, respectively.[11] The contrast effects of USPIO-CAs depend on the strength of the magnetic field, which can vary between scanners. Therefore, iso-intense USPIO-enhancement due to transient agent concentration in combination with scanner magnetic field strength might cause underestimation of ES. These two contrary facets of hyper- and hypo-signal changes on USPIO-enhanced $T_1$WIs may complicate the determination of enhancement magnitude and, therefore, regional intra-tumor tissue characteristics. This could also cause difficulty in the use of conventional diagnostic methods based on Gd-enhanced imaging, because the degree of malignancy and tissue type of brain tumors are determined based on the magnitude and texture of intra-tumoral Gd-enhancement. Previous studies on human intracranial tumors using a 3T-scanner found significantly greater changes in signal intensity as assessed using Gd-BCA compared with USPIO-CA. Qualitative analyses of lesion border delineation, internal morphology, and contrast enhancement also showed significant differences between the two agents, although no significant difference in enhancement volume of the lesions was reported between Gd- and USPIO-enhanced $T_1$WIs.[14] The present study demonstrates that the intra-tumoral ESs are also significantly different when measured using Gd-enhanced $T_1$WIs compared with USPIO-enhanced $T_1$WIs.

Our study histologically supports the use of USPIO-enhanced MRI for vascular bed imaging in E-phase after administration of CA. The USPIO-enhanced GRE $T_2$WIs exhibited strong, hypo-intense enhancement in the intra-tumoral area and vascular structures in E-phase. It has been reported that the transverse relaxivities of USPIO-CAs are significantly greater than the longitudinal relaxivities.[9,11] Therefore, GRE $T_2$WIs are sensitive to the presence of USPIO-CAs. Histologically, however, we detected few Prussian-blue-stained iron oxide particles in the extravascular

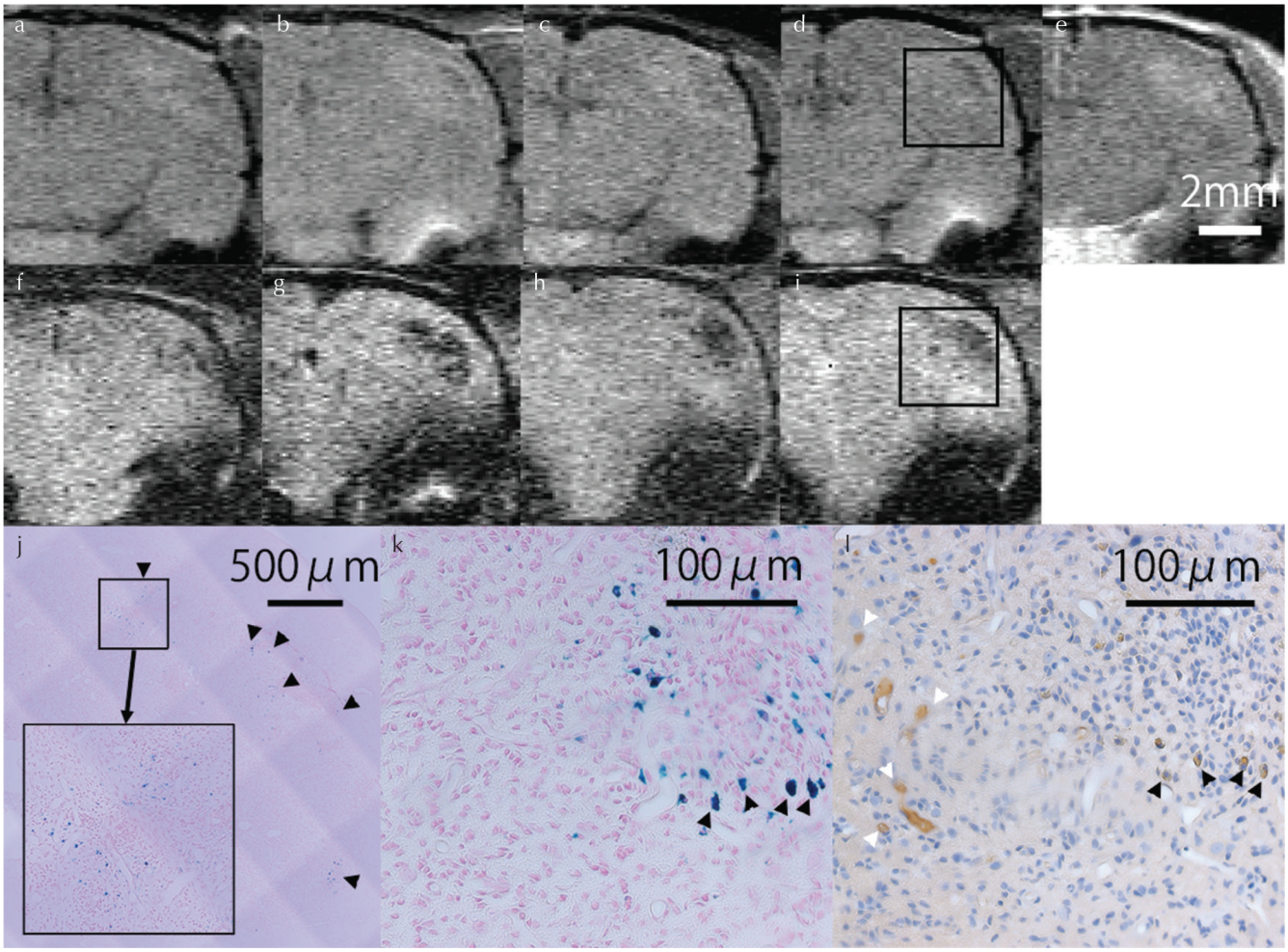


**Fig. 3** Time course of MR images and histopathologic specimens of a rat sacrificed following late-phase imaging. SE $T_1$WIs (top row) and GRE $T_2$WIs (bottom row) obtained (**a** and **f**) pre-contrast and at (**b** and **g**) 4 h, (**c** and **h**) 16 h, and (**d** and **i**) 63 h following administration of USPIO-CA. (**e**) Gd-enhanced SE $T_1$WI. The hypo-intense USPIO-enhancement in the early phase persisted in the late phase. The area where iron oxide blue dots are distributed on the Prussian-blue-stained specimen under low magnification (arrowheads in **j**) matches the area of hypo-intense enhancement (**j** corresponds to the square regions on the (**d**) SE $T_1$WIs and (**i**) GRE $T_2$WIs taken at 63 h after administration of USPIO-CA). The large square in **j** shows a high-magnification image of the small square region. In (**k**) the Prussian-blue- and (**l**) Iba1-stained specimens under high magnification, stained iron oxide particles are observed within the cellular space of Iba1-positive cells (arrowheads in **k** and **l**). Furthermore, Iba1-positive cells (thought to be microglia) consist of both iron-loaded microglia (arrowheads in **l**) and microglia without iron (white arrowheads in **l**). CA, contrast agent; GRE, gradient-recalled-echo; SE, spin-echo; $T_1$WI, $T_1$-weighted image; $T_2$WI, $T_2$-weighted image; USPIO, ultrasmall superparamagnetic iron oxide.

space of tumors. Presumably, in E-phase images, most of the administrated agent remained within the intravascular or extravascular space where it was removed by transcardial perfusion fixation. Contrast enhancement in brain tumors is produced by the presence of agent in both the intra- and extra-vascular spaces, which occurs due to leakage from vessels.[3] Since our ENU-induced glioma series included tumors with Gd-enhancement, BBB disruption must be occurred, allowing Gd-BCA to leak out.[13] It has been reported that dynamic perfusion MRI with USPIO-CAs provides a more accurate assessment of the vascular bed of brain tumors than Gd-BCA imaging, because USPIO-CA remains in the intravascular space in the E-phase after administration due to the larger particle size of the latter.[7,8,15]

Our histologic data support the results of these previous reports, however, the USPIO-CA in the intravascular space observed on E-phase images may explain why the hypo-intense USPIO-ES on GRE $T_2$WIs was statistically smaller than Gd-ES. Moreover, GRE $T_2$WIs can suffer from local magnetic inhomogeneities originating from pre-existing iron particle deposits and particular anatomical structures, such as mastoid air cells. In the present study, the three tumors with Gd-enhancement exhibited no USPIO-ES on GRE $T_2$WIs. This was caused by underestimation of ES on USPIO-enhanced GRE $T_2$WIs due to the large area of pre-existing intra-tumor hemorrhage and the periventricular anatomical location of the tumor. In addition, four tumors that were located near mastoid air cells exhibited severe signal

**Table 1** Comparison between USPIO- and Gd-enhancement size in the early phase following intravenous administration of USPIO contrast agent and number of tumors with USPIO-enhancement in the late phase

| Early-phase imaging | | 3–6 h following USPIO administration | | | | |
|---|---|---|---|---|---|---|
| | Enhancement pattern | Gd-enhancement | Hyper $T_1$ | Hypo $T_1$ | Sum of $T_1$ | Hypo $T_2$ |
| 10 tumors from early sacrificed rats | Number of tumors with enhancement | 10 | 3 | 7 | 7 | 9 |
| | Mean ES (min–max) ($mm^2$) | 34.19 (2.04–159.61) | 14.11 (0–127.63) | 5.19 (0–19.84) | 19.34 (0–147.47) | 24.42 (0–150.11) |
| Seven tumors from late sacrificed rats | Number of tumors with enhancement | 7 | 2 | 2 | 4 | 5 |
| | Mean ES (min–max) ($mm^2$) | 18.65 (1.84–53.80) | 0.67 (0–3.16) | 0.24 (0–1.00) | 0.91 (0–3.16) | 5.12 (0–27.84) |
| Total 17 tumors | Number of tumors with enhancement | 17 | 5 | 9 | 11 | 14 |
| | Mean ES ($mm^2$) | 27.79 | 8.58 | 3.15 | 11.75 | 16.47 |
| Wilcoxon signed-rank test vs. mean size of Gd-enhancement | *Z* | — | – 3.623 | – 3.622 | – 3.622 | – 3.465 |
| | *P* | — | <0.001 | <0.001 | <0.001 | 0.001 |
| Sum of $T_1$ USPIO-ESs vs. hypo $T_2$ USPIO-ES | *Z* | — | — | — | — | – 3.301 |
| | *P* | — | — | — | — | 0.001 |
| Late-phase imaging | Enhancement pattern | | Hyper $T_1$ | Hypo $T_1$ | Sum of $T_1$ | Hypo $T_2$ |
| Number of tumors with USPIO-enhancement | (Hours following USPIO administration) | 16–19 | 0/7 | 2/7 | 2/7 | 2/7 |
| | | 62–69 | 0/7 | 2/7 | 2/7 | 2/7 |

ES, enhancement size; Gd, gadolinium; Hyper $T_1$, hyper-intense $T_1$; Hypo $T_1$, hypo-intense $T_1$; Hypo $T_2$, hypo-intense $T_2$; min, minimum size of enhancement; max, maximum size of enhancement; Sum, summation; USPIO, ultrasmall superparamagnetic iron oxide.

loss on GRE $T_2$WIs and had to be excluded from analysis. These features of GRE $T_2$WIs could limit its use for clinical diagnostic imaging.

Late-phase MRI of the present study revealed intratumoral intensity changes (USPIO-enhancement). Histologic sections revealed iron-loaded microglia in the hypo-intense areas on GRE $T_2$WIs, suggesting that USPIO-IPs leaked slowly across the BBB or tumor vessel walls and then were taken up by microglia that were natively resident in the central nervous system. However, histologic sections also revealed that some microglia contained no iron oxide particles (Fig. 3). Protein corona on the surface of iron oxide nanoparticles has been suggested to influence the cellular uptake process of imaging agents.[11] One reason for the heterogenous distribution of USPIO-IP-containing microglia may be the heterogeneity of the vascular architecture, which delivers the agent to various regions within the tumor. Different types of microglia have different phagocytic activity and migration characteristics under the influence of the glioma,[12] which might also contribute to the heterogeneous distribution that we observed. If this enhancement could be used to evaluate the degree to which microglia are activated by tumors, it may provide insight into the clinical understanding of USPIO-enhanced MRI. It is also possible that L-phase USPIO-enhanced MR images could depict signal changes originating within the microglia, this suggestion warrants further study.

We found the time course of USPIO-enhancement to be in line with previous reports from clinical studies on humans and exogenous murine model studies,[6,7] which revealed peak $T_1$ enhancement in malignant tumors to peak 24–48 h after intravenous administration of ferumoxytol (which has a half-life of 10–14 h in humans[11]). Our study used carboxy-dextran coating for the particles, which has a half-life of 6–8 h in humans.[11] Since the half-life of the agent is much shorter in rats than humans,[16] the timing of E-phase scanning in the present study (6 h after administration of USPIO-CA) should have been sufficient for the tissue concentration of contrast agent to peak.

This study has several limitations that should be acknowledged. First, there was a mismatch between Gd- and USPIO-enhanced images, because they were obtained in different scan sets. This prevented objective comparison of the extent of intra-tumor enhancement between USPIO- and Gd-enhanced images through the use of a similarity coefficient such as Dice coefficient. Second, the section thickness was not identical between MR images and histologic specimens. Although we achieved excellent interrater agreement in terms of mean ES when comparing E-phase intra-tumor ESs on USPIO- and Gd-enhanced images, we should have used a three-dimensional acquisition MR sequence and co-registration tool to match the images. Third, the number of tumors with USPIO-enhancement was small, as was the observed ES in L-phase images. Although we administrated USPIO-CA at 10 times the usual clinical dose, maintaining a sufficient blood concentration to

enable transport across the BBB may have been difficult due to the reduced half-life of USPIO-CA in rats. Our results show that L-phase USPIO-enhanced MRI has the potential to detect USPIO-IP-loaded microglia, we used a 7T-scanner (Unity Inova VnmrJ 1.1c) with a magnet strength greater than that of scanners that are generally used in clinical settings. For evaluating L-phase USPIO-enhancement in a clinical setting, more sensitive and quantitative MRI techniques, such as quantitative susceptibility mapping, may be required.

## Conclusion

In summary, we demonstrate the use of intravenous administration of USPIO-CA for MRI in an ENU-induced endogenous glioma model, which eliminates unanticipated effects of implantation or grafting. The pattern and extent of USPIO enhancement on SE $T_1$WIs differed from those of Gd-enhanced images. Therefore, the use of USPIO-enhanced MRI in clinical settings should be carefully considered, because the diagnostic concepts will differ to those established for Gd-enhanced MRI for gliomas. We provide histological data supporting the use of E-phase USPIO-enhanced MRI for precise evaluation of intra-tumoral vascular bed volume and show that L-phase USPIO-enhanced MRI could be used to detect USPIO-IP-loaded microglia. However, L-phase cellular MRI with intravenous administration of the agent may present challenging in a clinical setting.

## Acknowledgment

This work was supported by a JSPS KAKENHI Grant Number 21591557.

## Conflicts of Interest

The authors declare that they have no conflicts of interest.

## References

1. Wen PY, Reardon DA. Neuro-oncology in 2015: progress in glioma diagnosis, classification and treatment. Nat Rev Neurol 2016; 12:69–70.
2. Johnson DR, Guerin JB, Giannini C, Morris JM, Eckel LJ, Kaufmann TJ. 2016 updates to the WHO brain tumor classification system: what the radiologist needs to know. Radiographics 2017; 37:2164–2180.
3. Zhang J, Liu H, Tong H, et al. Clinical applications of contrast-enhanced perfusion mri techniques in gliomas: recent advances and current challenges. Contrast Media Mol Imaging 2017; 2017:7064120.
4. Enochs WS, Harsh G, Hochberg F, Weissleder R. Improved delineation of human brain tumors on MR images using a long-circulating, superparamagnetic iron oxide agent. J Magn Reson Imaging 1999; 9:228–232.
5. Taschner CA, Wetzel SG, Tolnay M, Froehlich J, Merlo A, Radue EW. Characteristics of ultrasmall superparamagnetic iron oxides in patients with brain tumors. AJR Am J Roentgenol 2005; 185:1477–1486.
6. Muldoon LL, Sàndor M, Pinkston KE, Neuwelt EA. Imaging, distribution, and toxicity of superparamagnetic iron oxide magnetic resonance nanoparticles in the rat brain and intracerebral tumor. Neurosurgery 2005; 57:785–796.
7. Neuwelt EA, Várallyay CG, Manninger S, et al. The potential of ferumoxytol nanoparticle magnetic resonance imaging, perfusion, and angiography in central nervous system malignancy: a pilot study. Neurosurgery 2007; 60:601–611; discussion 611–612.
8. Beaumont M, Lemasson B, Farion R, Segebarth C, Rémy C, Barbier EL. Characterization of tumor angiogenesis in rat brain using iron-based vessel size index MRI in combination with gadolinium-based dynamic contrast-enhanced MRI. J Cereb Blood Flow Metab 2009; 29:1714–1726.
9. Weinstein JS, Varallyay CG, Dosa E, et al. Superparamagnetic iron oxide nanoparticles: diagnostic magnetic resonance imaging and potential therapeutic applications in neurooncology and central nervous system inflammatory pathologies, a review. J Cereb Blood Flow Metab 2010; 30:15–35.
10. Gahramanov S, Muldoon LL, Li X, Neuwelt EA. Improved perfusion MR imaging assessment of intracerebral tumor blood volume and antiangiogenic therapy efficacy in a rat model with ferumoxytol. Radiology 2011; 261:796–804.
11. Daldrup-Link HE. Ten things you might not know about iron oxide nanoparticles. Radiology 2017; 284:616–629.
12. Li W, Graeber MB. The molecular profile of microglia under the influence of glioma. Neuro-oncology 2012; 14:958–978.
13. Doblas S, He T, Saunders D, et al. Glioma morphology and tumor-induced vascular alterations revealed in seven rodent glioma models by in vivo magnetic resonance imaging and angiography. J Magn Reson Imaging 2010; 32:267–275.
14. Dósa E, Guillaume DJ, Haluska M, et al. Magnetic resonance imaging of intracranial tumors: intra-patient comparison of gadoteridol and ferumoxytol. Neuro-oncology 2011; 13:251–260.
15. Gambarota G, Leenders W, Maass C, et al. Characterisation of tumour vasculature in mouse brain by USPIO contrast-enhanced MRI. Br J Cancer 2008; 98:1784–1789.
16. Troprès I, Lamalle L, Péoc'h M, et al. In vivo assessment of tumoral angiogenesis. Magn Reson Med 2004; 51:533–541.